

## Low-threshold lasing and broad-band multiphoton-excited light emission from Ag aggregate-adsorbate complexes in microcavity

VLADIMIR P. DRACHEV‡, WON-TAE KIM†, VLADIMIR P. SAFONOV§, VIKTOR A. PODOLSKIY†, NIKOLAI S. ZAKOVRYASHIN§, ELДАР N. KHALIULLIN†, VLADIMIR M. SHALAEV† and ROBERT L. ARMSTRONG†

†Department of Physics, New Mexico State University, Las Cruces, NM 88003, USA

‡Institute of Semiconductor Physics, Novosibirsk, 630090, Russia

§Institute of Automation and Electrometry, Novosibirsk, 630090, Russia

(Received 1 April 2001; revision received 16 June 2001)

**Abstract.** A novel class of composites for optics, microcavities doped with metal fractal aggregates, is studied. Lasing and broad-band Stokes and anti-Stokes emission from (Ag colloidal aggregates)/(adsorbed molecules)/(microcavity) composite at low-intensity cw and pulse laser excitation has been found. At 633 nm cw excitation wavelength the emission spectrum contains many peaks, spanning a range from wavelength 200 nm to 800 nm. Experiments with pulse excitation of Ag/dye/microcavity composite show that the duration of the observed broad-band anti-Stokes emission significantly exceeds the pump pulse duration, dye molecule fluorescence time, and relaxation times in silver particles. It may be interpreted as a luminescence governed by long-living triplet states of dye molecules. These observations were made possible by use of a fractal-microcavity composite, where coupling the localized plasmon modes in fractal aggregates with microcavity resonances is provided. The important role of multiphoton resonant transitions between discrete states of a finite-size metal particle in enhanced local fields is shown. Analysis, based on the model of a spherical potential well, shows that the observed spectra contain fingerprints of the quantum size effect.

### 1. Introduction

Since the discovery of surface-enhanced Raman scattering [1], the optical properties of metal-molecule complexes have attracted considerable interest [2–4]. Molecules adsorbed onto nanoscale roughened metal surfaces or nanostructured metal colloids produce a millionfold increase in the intensity of Raman, absorption, and fluorescence emission [3]. Second-harmonic generation at a silver–air interface is enhanced by surface roughness and it is accompanied by a broad luminescence background extending far beyond the anti-Stokes side of the second harmonic [5]. Nonlinear Raman scattering (termed hyper-Raman scattering) [6–9] and two-photon excited luminescence of complexes (dye molecule)/(silver colloidal aggregate) [10] are also facilitated by the surface-enhanced effect. The question

of whether electronic transitions of interest include pure molecular states of the adsorbate or if metal states are also involved in the process via a charge-transfer mechanism is still under discussion and may depend on experimental conditions [4, 7, 11–13]. However, it is commonly recognized that all the aforementioned phenomena are accompanied by strongly enhanced electric fields in the vicinity of the metal structure via the excitation of resonant surface-plasmon modes [3, 14].

Far greater enhancement of Raman scattering may be achieved at extremely low pump intensity by coupling collective plasmon modes with microcavity resonance modes in so-called fractal-microcavity composite media [15]. Furthermore, lasing at low intensity has been reported for a dye-Ag colloid system placed within a cylindrical microcavity [15].

It is of great interest to study applications of fractal-microcavity composites to the enhancement of various optical responses. This paper reports the results of studies of a number of radiation processes, dramatically enhanced in a composite (Ag aggregate/adsorbate/cylindrical microcavity). Enhanced luminescence and lasing from an Ag/dye/microcavity and broad-band multiphoton-excited emission from Ag aggregate-adsorbate complexes seeded into a cylindrical microcavity under cw and pulsed excitation have been observed. In the latter, sodium citrate and dye molecules were used as adsorbates. Under 633 nm excitation, the emission spectrum contains discrete peaks, spanning a wavelength range from 200 nm to 800 nm. Quasiperiodic structures may be distinguished in the broad-band spectrum. Some structures may be attributed to modes of a coupled resonator formed by morphology-dependent resonances (MDRs) of the microcavity and nanoscale resonances of the fractal aggregates embedded within the microcavity. Other spectral periods may be attributed to optical properties of the material inside the coupled resonator. The duration of the broad-band emission from Ag/dye/microcavity composites for pulsed excitation, which exceeds the times of laser excitation and relaxation for dye fluorescence and the times of electron and thermal processes in metal particles, may be interpreted as luminescence governed by long-living triplet states of the dye molecules.

The intensity of multiphoton-excited emission is comparable with that of Raman emission at low cw pump intensities provided by a  $20 \text{ W cm}^{-2}$  HeNe laser. One cannot attribute observed spectral emissions to hyper-Raman processes from purely molecular transitions. In this paper, we suggest a possible explanation in terms of: (i) the theory of discrete energy states and saturation effects in the degenerate electron gas in spherical metallic particles [16]; (ii) the discovery and theory of light emission from metal particles under inelastic electron tunnelling [17, 18]; and (iii) the theory of charge-transfer states of molecule-metal complexes [11, 13]. The discrete spectrum observed in the anti-Stokes region is inferred to result from two- and three-photon excitation of metal states followed by radiative decay, via surface states coupled with molecular transitions, into unoccupied discrete states of metal nanoparticles. Interpretation of the spectrum under these assumptions is in qualitative agreement with the observed experimental spectrum. The huge enhancement of multiphoton optical phenomena observed in our experiments occurs because of high local fields of the coupled fractal-microcavity modes and resonant states of the colloid-adsorbate complex.

## 2. Experimental setup and samples preparation

The metal nanostructures used in our experiments consisted of several types of silver colloidal aggregates. One of the colloids was produced using the Lee-Meisel method [19], involving the reduction of silver nitrate by an aqueous solution of sodium citrate; sodium citrate molecules adsorbed on the silver particles were present in concentrations of  $5 \times 10^{-4}$  M. The average radius of these Ag(LM) monomers was  $R_0 \sim 11 - 12$  nm while the aggregates, comprising  $N = (R_c/R_0)^D \sim 10^3$  monomers, had radii  $R_c \sim 1 \mu\text{m}$ , where  $D$  is the fractal dimension. A transmission electron microscope image of a typical fractal cluster is shown in figure 1(a) insert. Analysis of many similar images yields a fractal dimension  $D \approx 1.77$ , in excellent agreement with the theoretical value of 1.78.

The second method of sample preparation used collargol, which is a mixture of silver with proteins that stabilize the hydrosol. Diameters of silver monomers in a water solution of collargol were  $\sim 10$  nm, and fractal clusters contained hundreds of monomers.

A third colloid solution, Ag(PVP) was prepared according to [20]. The silver is reduced by a monomeric residue of polyvinylpyrrolidone (PVP) in ethanol. The average diameter of Ag microparticles is  $d_{av} = 13 \pm 2$  nm and the fractal aggregates have sizes up to  $0.5 \mu\text{m}$ .

A fourth method [21] involved reduction of  $\text{AgNO}_3$  by a mixture of  $\text{FeSO}_4$  and  $\text{Na}_3(\text{cit})$ . Concentrations of all solutions 120 times less than in [21] were used, which corresponds to  $1.7 \times 10^{-3}$  M of silver. The coagulating fractal aggregates range up to several microns in size, the particle diameter is  $d_{av} = 12 \pm 3$  nm, and the average particle separation is about 1 nm.

Composites are formed when aggregates are seeded into a dielectric microcavity, consisting of a hollow quartz tube of outer diameter 1 mm, inner diameter 0.7 mm. Sodium citrate or rhodamine 6G (R6G) molecules were adsorbed on silver particles; green ( $\lambda = 543.5$  nm) and red ( $\lambda = 632.8$  nm) cw HeNe lasers, and a pulsed Nd:YAG laser and its second harmonic were used as excitation sources.

The schematic experimental arrangement, shown in figure 1(b), has been described elsewhere [15]. The pump laser is focused near the inner rim of the cylindrical microcavity in a plane perpendicular to its axis, ensuring efficient coupling to morphology-dependent resonances (MDRs). The focal plane beam diameter was  $35 \mu\text{m}$  for the green HeNe laser and  $50 \mu\text{m}$  for the red one. The radiation from aggregated colloids in the microcavity is observed at 90 degrees to the incident radiation. The light is gathered by the collection optics and input to an Acton imaging spectrograph fitted with either a 300 or an 1800 groove  $\text{mm}^{-1}$  grating. The 1800 groove  $\text{mm}^{-1}$  grating provided a spectral resolution of 0.028 nm (full width at half maximum). Spectrally analysed emissions are recorded using a Princeton Instruments CCD detector. In other experiments, a double monochromator with a 600 groove  $\text{mm}^{-1}$  grating (dispersion  $1.6 \text{ nm mm}^{-1}$ ) and photomultiplier detection were used.

To avoid possible spectral contamination by laser plasma lines, a laser filter was placed before the sample. A blocking notch filter was inserted after the sample to minimize the amount of stray light at the pump wavelength reaching the CCD. Composite spectra were obtained by superposing eight individual overlapping spectral regions from 200 nm to 800 nm using long- or short-pass filters placed after the sample to isolate each region. Individual spectra were combined by matching the relative values of peak intensities in the overlapped portions accounting for the

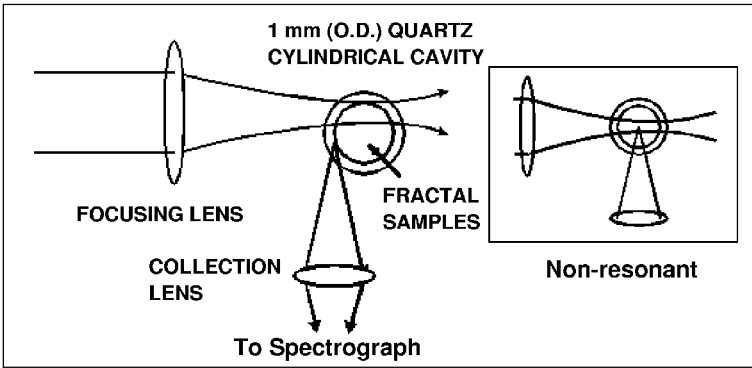
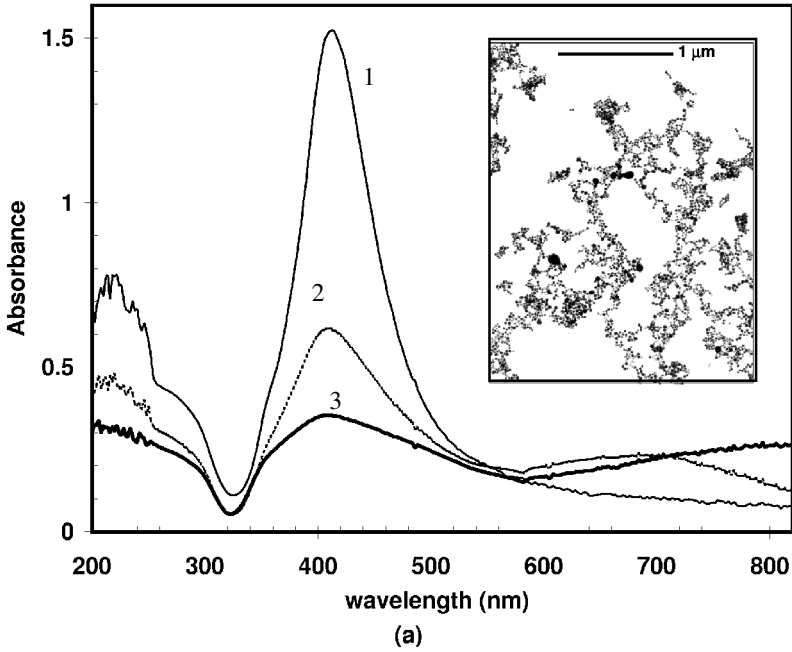


Figure 1. (a) Absorption spectra (1. nonaggregated mono-dispersed colloid, 2. small fractal aggregates, 3. large fractal aggregates), and TEM image of fractal aggregate (inset). (b) Experimental setup.

spectral sensitivity of the CCD. This procedure eliminates possible spectral contamination by grating ghosts or overlapping diffraction orders. Finally, spectra for aggregated and nonaggregated samples were compared for each spectral trial.

### 3. Elastic scattering and absorption

Elastic scattering of a laser beam passed through the outer edge of the empty cylindrical tube exhibits well-defined MDR angular structure consistent with

modes of a cylindrical microcavity with an outer diameter of 1 mm. Alternatively, when the beam is passed through the inner edge of the empty tube, the intensity of the MDR angular structure is significantly reduced. However, using the latter geometry and filling the tube with a colloidal solution again results in strong elastic scattering with a clearly resolved MDR structure. Most of our experiments were performed using this illumination geometry.

To study the wavelength dependence of elastic light scattering in the Ag(col-largol)/microcavity system, a tunable cw dye laser was used. Three characteristic MDR mode spacings in the elastic scattering spectrum were found. The minimum period of  $2 \text{ cm}^{-1}$  closely approximates the theoretical intermode spacing of  $\Delta\nu = (1/2\pi r)((n^2 - 1)^{-1/2} \tan^{-1}(n^2 - 1)^{1/2})$ , calculated for a quartz microcavity of radius  $r = 0.5 \text{ mm}$  and refractive index  $n \approx 1.46$ . Two other MDR spacings of  $13 \text{ cm}^{-1}$  and  $37 \text{ cm}^{-1}$  were also found to depend on the illumination geometry.

Figure 1(a) shows absorption spectra of solutions containing citrate molecules adsorbed on Ag(LM) silver particles in different stages of aggregation. The aggregation is accompanied by a decrease of the single particle plasmon peak near 410 nm and growth of the long-wavelength wing is apparent above 700 nm. Analogous absorption spectra are observed for monomer and aggregated silver colloids of the other types. Experimental [15] and theoretical [14] studies reveal that the optical enhancement increases dramatically with aggregation of particles into clusters.

#### 4. Experiments with 543.5 nm excitation

Consider first experiments with R6G/Ag(LM)/microcavity composite under 543.5 nm excitation. The concentration of R6G was  $5 \times 10^{-7} \text{ M}$ , which corresponds to approximately 250 R6G molecules per each monomer at the concentration of Ag particles ( $R_0 = 11.310^{12} \text{ nm}$ ). Figure 2 illustrates the huge increase in the intensities of emission peaks for R6G/Ag aggregates/tube composites in comparison with monomer colloid solutions with or without R6G. (Different neutral density filters were used for recording these three spectra; enhancement factors are discussed below.) The largest peaks are centred within a narrow spectral region near  $\lambda = 600 \text{ nm}$  with a bandwidth of approximately 6 nm. At low resolution (figure 2, grating  $300 \text{ gr mm}^{-1}$ ), R6G/Ag/tube emission in the range of 575–650 nm contains three characteristic spacings between peaks. One spacing of approximately  $13 \text{ cm}^{-1}$  coincides with the second spacing observed for the elastic scattering, while the other two observed spacings are different, 54 and  $110 \text{ cm}^{-1}$ . Closely spaced but spectrally distinct modes are found in the high-resolution spectrum ( $1800 \text{ gr mm}^{-1}$ ); these intermode spacings are essentially identical to those for elastic scattering ( $2 \text{ cm}^{-1}$ ). The observed width of a single peak,  $\delta\lambda = 0.04 \text{ nm}$ , which closely approximates our instrumental width, allows estimation of a lower bound for the MDR quality factors,  $Q > \lambda/\delta\lambda = 1.5 \times 10^4$ .

A weak luminescence with a spectral width of 30 nm was observed from the R6G/microcavity composite without silver aggregates. The luminescence intensity grows when Ag colloid monomers are added and further increases with aggregation of the colloid. Increased luminescence accompanying photostimulated aggregation of silver particles was observed in [22]. Luminescence enhancement resulting from fractal aggregates was  $10^5$ . The multiplicative enhancement provided by Ag aggregates/microcavity composites was estimated to be  $10^9$ .

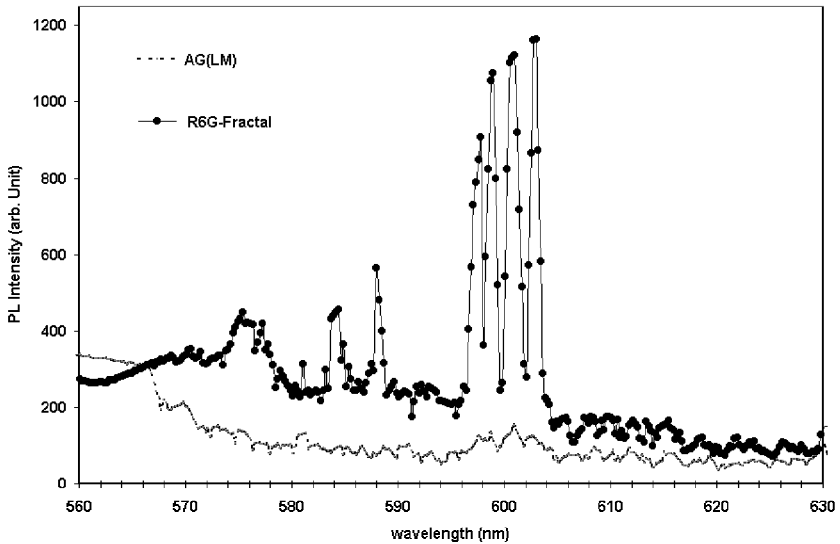


Figure 2. Emission spectra of the composites R6G/Ag(Lee-Meisel)/tube (upper trace), Ag(Lee-Meisel)/citrate/tube (lower spectrum) at 0.75 mW excitation at 543.5 nm. Neutral density filters OD = 5 were used for the upper spectrum recording. Grating 300 gr mm<sup>-1</sup>.

The emission intensity of different spectral components was studied as a function of the pump intensity. It was found that this dependence is linear for low excitation intensities for all components. However, when the pump intensity exceeds some critical value in the range between 20 and 50 W cm<sup>-2</sup>, some peaks grow dramatically, exhibiting a lasing threshold dependence. The threshold power for  $\lambda_L = 543.5$  nm He-Ne laser excitation is as small as  $2 \times 10^{-4}$  W.

In these experiments, the spatial-temporal structure of luminescent emission from a microcavity was investigated as a function of position along its vertical cylindrical symmetry axis; this was accomplished by directly imaging the microcavity on the (vertical) entrance slit of an imaging spectrograph. The emission was found to be confined within an approximately  $\sim 50$   $\mu\text{m}$  region of the cylinder, which contained the incident pump light; moreover, emission from this region exhibits angular patterns characteristic of microcavity MDRs. The spectral profiles of the lasing peaks were also observed to be time dependent during cw laser pump excitation. Specifically, when the detector integration time was greater than one second, a smoothing of the lasing spectrum was observed; i.e. the spectrally sharp lasing peaks merged into intense, but spectrally broad, features. It is suggested that this is primarily due to pump laser-induced heating which, in turn, induces changes in the refractive index and, ultimately, in MDR resonant wavelengths.

Thus, the spectral, threshold, and spatial dependence confirm the lasing nature of the observed emission. It is noteworthy that the R6G concentration was only  $5 \times 10^{-7}$  M in these experiments, three orders of magnitude lower than that for conventional dye lasers with an external cavity and three orders of magnitude lower than that for a microdroplet laser without silver fractal aggregates [23, 24].

In the present experiments, the minimum R6G concentration that results in lasing can be as low as  $10^{-8}$  M. These findings suggest that the lasing effect is due to dye molecules adsorbed on the surface of silver aggregates. This conclusion is also supported by the fact that increasing the R6G concentration to  $10^{-5}$  M does not result in additional growth of the lasing peak intensities; the additional dye concentration is apparently not adsorbed onto the silver particles, but remains in solution as free molecules, where it does not effectively contribute to the enhanced lasing effect.

It should be noted that peaks in figure 2 are shifted to the long-wavelength wing of the R6G luminescence band. As previously reported, such a shift is characteristic of the spectra of both the R6G cw microlaser [23] and the pulsed microlaser [25]. The authors of [23, 25] suggest that this effect is caused by the reduction in R6G absorption with increasing wavelength. In our experiments, there is an additional important reason for the observed shift. Namely, the fractal resonance-induced enhancement factor for the local electric field,  $G = |\epsilon - \epsilon_h|^2 / (3\epsilon_h\epsilon_m'') \propto \lambda$ , is larger for longer wavelengths [14] (where  $\epsilon = \epsilon_m' + i\epsilon_m''$  and  $\epsilon_h$  are the dielectric functions for silver nanoparticles and the host medium (water), respectively). This point is also illustrated in figure 3, depicting spectra obtained

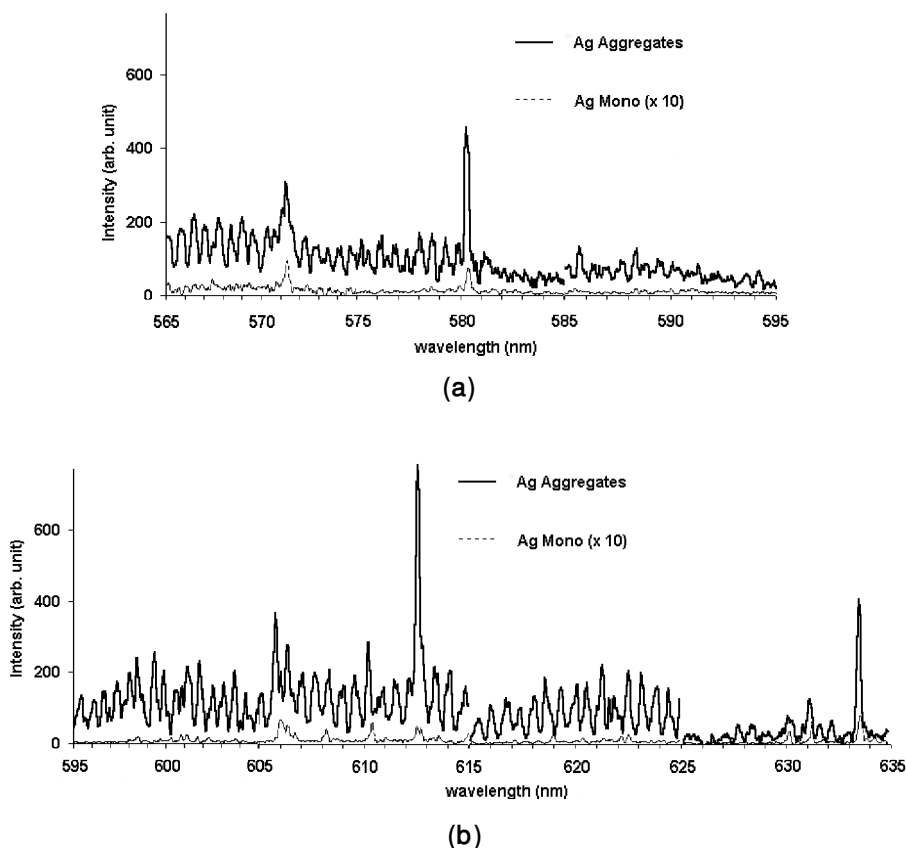


Figure 3. As figure 2, but with grating  $1800 \text{ gr mm}^{-1}$  and for other alignments (a) 565 to 595 nm, (b) 595 to 635 nm.

for the same solutions as for figure 2, but with an  $1800 \text{ grmm}^{-1}$  grating and for other alignments of the tube. One can see a broad luminescence of R6G shifted to the long-wavelength range relative to the usual yellow R6G luminescence. The characteristic feature of this spectrum is the presence of quasiperiodic peaks with a minimal intermode spacing of  $2 \text{ cm}^{-1}$  and an additional spacing of approximately  $16 \text{ cm}^{-1}$ , which is close to the spacing of  $13 \text{ cm}^{-1}$  discussed above. Note, that the intensity of peaks is modulated by a larger period of approximately  $300 \text{ cm}^{-1}$ .

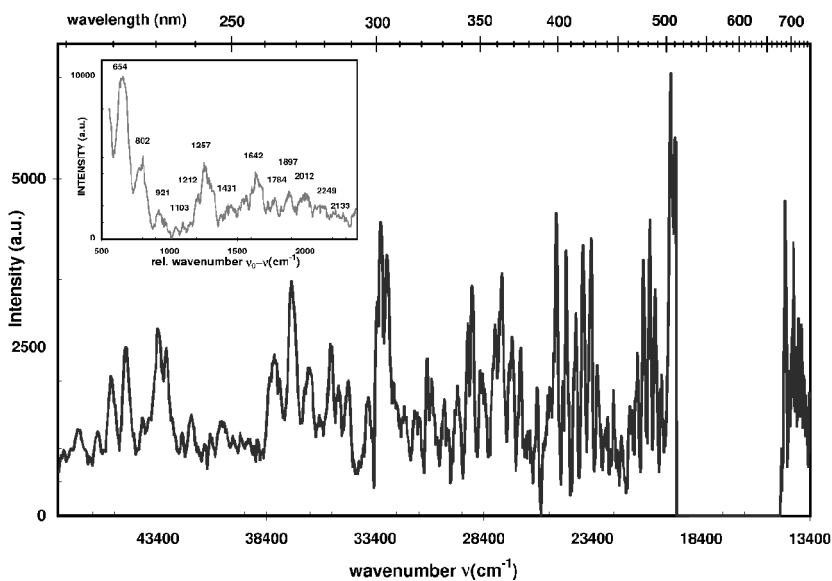
The three strongest peaks in figure 3 can be attributed to surface-enhanced Raman scattering on sodium citrate molecules; we discuss Raman spectra below. However, here we note that the multiplicative enhancement for the Raman peak at  $580 \text{ nm}$  ( $1160 \text{ cm}^{-1}$ ), which may be  $10^9$  or greater, was found for R6G/citrate/(Ag aggregates)/microcavity composites relative to sodium citrate solution in [15]. Possibly, the presence of R6G facilitates the enhancement of Raman emissions in addition to the fractal and microcavity enhancements.

It is interesting that a number of peaks in figure 3 were also observed in citrate/Ag/microcavity composites. Note that nonlinear scattering under low-intensity cw excitation of a microdroplet was observed in [26]. The questions to address here are: what is the scattering medium and what are the processes responsible for emission of the spectral peaks, observed from Ag/adsorbate/microcavity composites? To answer these questions experiments were performed with other excitation wavelengths and with pulsed excitation.

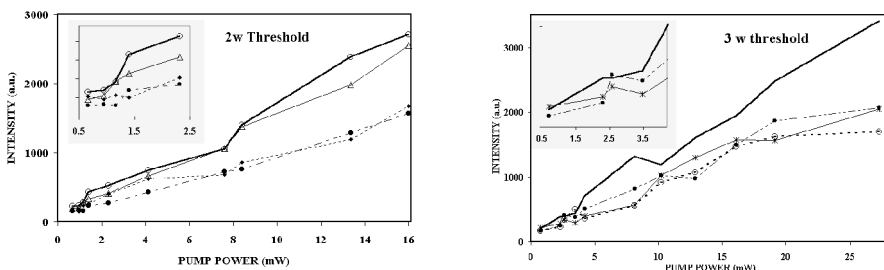
## 5. Experiments with 633 nm excitation

Experiments show that the  $632.8 \text{ nm}$  HeNe laser excites strong Raman scattering and anti-Stokes emission at the condition of a spectral overlap with the long-wavelength wing of the absorption spectrum for fractal aggregates, so that strong coupling to surface plasmon modes occurs [14, 15].

Figure 4(a) shows a low-resolution spectrum obtained using a  $300 \text{ grmm}^{-1}$  grating. The spectra obtained are extremely broadband, spanning a range from at least  $200$  to  $800 \text{ nm}$ ; spectra were not recorded outside of this range because of the degraded response of the spectrometer and the CCD. The spectrum on the anti-Stokes side consists of several groups of well-resolved lines in the  $\nu_0$  to  $2\nu_0$  region with spectral resolution from  $5$  to  $20 \text{ cm}^{-1}$ . In the  $2\nu_0$  to  $3\nu_0$  region, CCD ‘pixel’ errors are larger,  $47 \text{ cm}^{-1}$ , and spectral structures are poorly resolved or unresolved. The insert displays the Stokes-side spectrum, which contains Raman peaks and a broad emission band. For comparison, spectra were also obtained for (i) a concentrated sodium citrate solution without colloid, (ii) fractal aggregates with citrate in a cuvette, and (iii) fractal aggregates with citrate seeded into a microcavity. Raman emission was observed in all cases, but multiphoton emission occurs only in fractal-microcavity composites, which provide the greatest enhancement. The measured enhancement factor for Raman scattering,  $G^{(RS)}$ , is defined as the product of two measured RS intensity ratios: from citrate adsorbed on fractal aggregates and from a concentrated sodium citrate solution without colloid,  $I_f/I_w \sim 10^5 - 10^6$ ; and from fractal solutions with and without a microcavity,  $I_{f-mc}/I_f \sim 10^4$ . The RS enhancement factor with a microcavity,  $G^{(RS)} \sim 10^9 - 10^{10}$ , reveals up to four orders more than the *average* (macroscopic) RS enhancement on rough metal surfaces or colloidal aggregates without a microcavity, which is known to be  $\sim 10^6$  [2, 3]. Local field enhancement in a



(a)



(b)

Figure 4. (a) Emission spectrum of the composite Ag(Lee-Meisel)/citrate/tube and Raman Stokes spectrum of sodium citrate at 633 nm excitation (inset). (b) Intensity dependence for several spectral lines.

microcavity containing fractal aggregates results in up to four orders more RS enhancement.

Note that Raman scattering from a pure citrate solution (without Ag colloid) placed in a microcavity shows no enhancement with respect to bulk measurements. It is concluded that in the presence of a high scattering medium (aggregated colloid) the coupling to MDR modes increases; MDR modes may also have a different radial field distribution in this case. In the case of a transparent medium, the penetration depth of microcavity modes is much less than the size of the tube wall and overlap between the field and the medium is negligible. However, a highly scattering medium placed in a microcavity may result in secondary sources of radiation in the vicinity of the inner surface of the tube, and the formation of cavity

modes. This may be the reason why optimal alignment for this case requires the beam to be focused near the inner rim of microcavity.

Investigations of the intensity dependence of the anti-Stokes emissions (figure 4b) show that, as pump power increases, the intensity dependence (initially nonlinear) becomes quasi-linear for pump powers above approximately 2 mW. The dramatic local field enhancement in fractal-microcavity composites and the resonant character of the excitation processes can lead to an unusual intensity dependence, because of saturation effects.

To estimate the contribution of hyper-Raman emission from pure molecular transitions to the anti-Stokes spectrum (see the Discussion section), we specifically compare the emission spectrum with Raman peak positions, and estimate the hyper-Raman/Raman intensity ratio.

According to previous studies [27, 28], SERS spectra from sodium citrate on Carey-Lea citrate-stabilized silver hydrosol show a weak band near  $650\text{--}660\text{ cm}^{-1}$ , no band near  $1640\text{--}1660\text{ cm}^{-1}$ , and a dominant band at  $1400\text{ cm}^{-1}$ . As described above, silver sol was prepared using the Lee-Meisel method with addition of NaCl. In this case, sodium citrate, a salt of a propanetricarboxylic acid  $\text{C}_6\text{H}_8\text{O}_7$ , exhibits a modified SERS spectrum (see figure 4a insert) characteristic of some carboxylic acids, such as substituted acetic [29] and formic acids [30]. The spectral signature of the modified spectrum includes a reduced intensity of the  $\text{COO}^-$  vibration near  $1410\text{ cm}^{-1}$  (the dominant band in bulk spectra) and increased intensity of Raman bands near  $1640\text{ cm}^{-1}$  (C=O stretch), with the ratio of intensities strongly depending on adsorption details. Previous studies of SERS spectra of different carboxylic acids [27–32] exhibit slightly different spectra for the same adsorbate and equivalent SERS spectra for different adsorbates. Explanations for the modified spectrum include geometric orientation effects of the adsorbate with respect to the metal surface [29, 32] and chemical transformation during formation of the adsorbate–metal complex [30], so that the spectra depend on sol preparation and age. The presence of  $\text{Cl}^-$  results in an intense  $1636\text{ cm}^{-1}$  band and an unobservable  $1400\text{ cm}^{-1}$  band, indicating that  $\text{COO}^-$  has been desorbed from the silver surface and the molecules are adsorbed mainly via the OH group [31].

Summarizing, the comparison of spectral lines near  $2\nu_0$  with Raman peaks near  $\nu_0$ , reveal that only a small number can be interpreted as hyper-Raman emission from adsorbate molecules: specifically, two peaks (at  $800$  and  $933\text{ cm}^{-1}$ ) have shifts from  $2\nu_0$  approximately equal to the SERS shifts  $807$  and  $921\text{ cm}^{-1}$ ; in addition, a number of other peaks may be regarded as overtones of the Raman fundamentals (e.g.  $2 \times 1256\text{ cm}^{-1}$ ,  $2 \times 1642\text{ cm}^{-1}$ ,  $3 \times 1256\text{ cm}^{-1}$ ). Thus, although we can identify a fraction of peaks as resulting from surface-enhanced Raman scattering, many peaks in the broad-band spectrum may not be attributed to either Raman or hyper-Raman scattering from adsorbate molecules (see discussion below). This conclusion is also supported by experiments using pulsed excitation.

## 6. Experiments with pulsed excitation

A R6G/Ag/microcavity composite was irradiated by a 14 ns Nd:YAG pulse at  $\lambda_L = 1064\text{ nm}$ . The intensity of the excitation at the microcavity was  $I \lesssim 18\text{ MW cm}^{-2}$ . The 1.26 mm outer, 0.98 mm inner diameter quartz tube was filled with Ag(PVP) or Ag(Carey-Lea) colloid with (or without)  $10^{-6}\text{ M}$  R6G. Emission was detected with the help of a double monochromator and a photomultiplier.

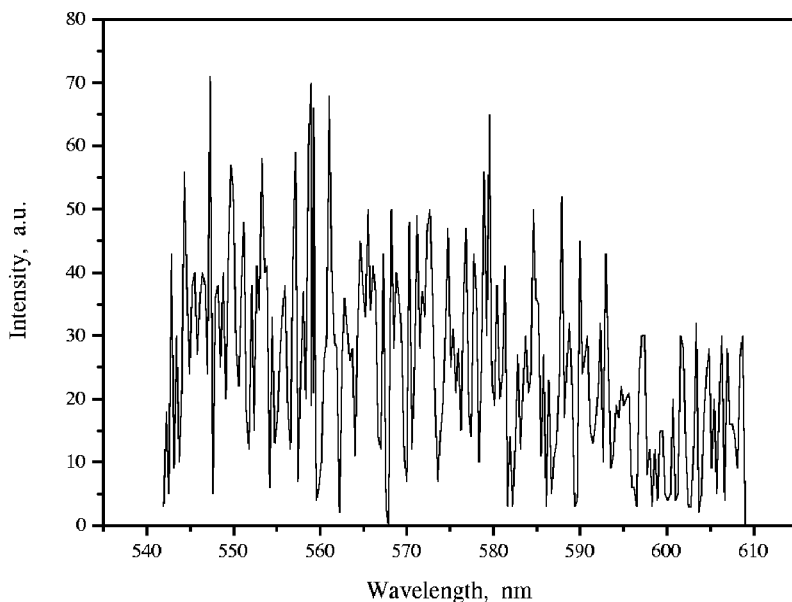


Figure 5. Fragment of luminescence spectrum of the composite R6G/Ag(Carey-Lea)/tube, at 1064 nm pulsed excitation.

Broad-band anti-Stokes emission was observed from R6G/(Ag Carey-Lea aggregates)/microcavity composites in the 410–650 nm range; the boundaries of this range are limited by monochromator and photomultiplier characteristics. Part of the spectrum, containing many peaks, is shown in figure 5. Peak intensities are approximately the same as in the range 410–650 nm. The minimal spectral width of these peaks was limited by the instrumental resolution of approximately  $10\text{ cm}^{-1}$ . Dependence of the broad-band emission on pump power is nonlinear. The observed emission spectrum is much wider and more intense than luminescence from R6G molecules in solution without silver colloid. An ethanol solution of  $5 \times 10^{-4}\text{ M}$  R6G under 1064 nm excitation emits in the range 540–610 nm with a maximum at 565 nm. The enhancement factor of the R6G/Ag/microcavity composite emission relative to the R6G/microcavity emission at 565 nm in the band  $\Delta\lambda = 3.2\text{ nm}$  was found to be  $5 \times 10^2$ . The enhancement factor for the blue range is much greater. Only very weak emission is observed from Ag/microcavity composites without R6G.

Note that the emission spectrum described here differs significantly from the two-photon excited luminescence of R6G/(Ag aggregates) in a cuvette under pulsed excitation, as reported in [10]. The continuous luminescence band in the range 540–700 nm lie in a different region (than two-photon excited luminescence from R6G) and their maxima are displaced over a rather wide spectral range from substance to substance. Based on these facts the authors of [10] interpreted the observed band as sensitized luminescence of silver particles.

The broad-band anti-Stokes emission from the R6G/Ag(PVP)/microcavity composite spans the region from 540 nm to 600 nm. The difference in spectral widths in composites with two colloids is possibly due to the difference in compositions of the two studied colloids.

The excitation of the R6G/Ag(Carey-Lea)/microcavity composite by a laser pulse at  $\lambda_L = 532$  nm results in luminescence in the range 510–620 nm. The peak spectral structure is characteristic of this emission as well as of other emissions from the microcavity. The pulse duration of this luminescence does not exceed the temporal resolution of our detector (20 ns).

The pulse duration of anti-Stokes emission for excitation of R6G/Ag(Carey-Lea)/microcavity at 1064 nm grows with pump intensity and may be more than 1  $\mu$ s. This time is much longer than the R6G fluorescence time ( $\sim 10^{-9}$  s) and relaxation times in Ag nanoparticles ( $\sim 10^{-12}$  s), including the thermal relaxation ( $\sim 10^{-10}$  s).

The data summarized here provide evidence that we have observed multiphoton-excited, multiplicatively-enhanced luminescence of R6G/Ag complexes in the microcavity. The observation of enhanced luminescence shows that the adsorbate molecules in these colloids are placed at a certain distance from the metal surface. According to [3, 33], surface-enhanced Raman scattering is effectively excited for molecules touching the metal surface, whereas surface-enhanced luminescence occurs for slightly more distant molecules. Observation of the long-time emission shows that triplet levels of R6G molecules are the reservoir of energy for the broad-band luminescence. Note that the triplet states usually quench luminescence of dye molecules in solution and decrease the gain coefficient in dye lasers.

## 7. Discussion

A characteristic feature of microcavity emissions observed in these experiments is the spectral structure of the peaks. First, note that some spectral spacings in this structure (2 and 13  $\text{cm}^{-1}$ ) coincide with the MDR spacings for a 1 mm tube filled with silver aggregates, having a wall thickness of 0.15 mm and refractive index of 1.45 (the angle of incidence is  $\approx 45^\circ$ ). Since this structure depends on optical alignment of the tube, it can be identified with microcavity MDRs, further implying that the emission is coherent. Taking into account the low excitation power and low dye concentration, it is believed that coherence is possible because the coupled cavities, formed by the nanoresonators (fractal plasmon mode with size  $\approx \lambda$ ) and the microcavity, result in the dramatic enhancement of radiative processes.

The enhancement of radiative processes by the cavity quantum-electrodynamic modification (Purcell effect [34]) was demonstrated in Fabry–Perot micro-nanoresonators and in microdroplets [35–38]. Stimulated emissions at extremely low excitation and anomalously high gain coefficients were found for dye molecules in a microcavity with size  $\lambda/2$  [35]. The reduction of dimensionality of the mode ensemble in the microcavity results in a collective state of emitters inside the cavity. Multiple scattering of the EM field in a fractal cluster results in the formation of high-quality modes, localized at a scale of  $\lambda$  or less. In these experiments emitters are inside a fractal nanoresonator and simultaneously inside a microcavity. The density of emitters in the nanoresonator is high. The emission in a (fractal cluster)/adsorbate system arises from the coupling of closely placed emitters to a relatively small number of zero-point field modes. This radiation may be collective and coherent. Different fractal aggregates inside the microresonator have maximum quality factors at different wavelengths, therefore the emission

spectrum of an ensemble is broadened inhomogeneously. The enhancement of exciting fields involved in a multiphoton process provides an additional contribution to the overall enhancement and the figure of merit for the radiation [22, 39].

As mentioned above, one of the contributing processes is enhanced hyper-Raman scattering. Following [7], the ratio of hyper-Raman/Raman intensity may be estimated from the ratio of RS and HRS intensities in bulk solution, which is  $I_{HRS}/I_{RS} \sim 10^{-14}$ – $10^{-15}$  for the pump intensity,  $I \sim 20 \text{ W cm}^{-2}$ , used in these experiments. For pure molecular transitions, the cross-sections are assumed to be unchanged; hence, this ratio may increase only as a result of the local field enhancement in fractal-microcavity composites.

The enhancement of molecular Raman scattering in a fractal solution is a well-established factor and is of the order  $10^6$ .

The HRS fractal enhancement  $G_{fract}^{(n)}$  is defined as the average of a ratio (raised to a proper power) of local to external fields. Following the general approach described in [14],  $G_{fract}^{(n)}$  is expressed in terms of  $X(\omega)$  and  $\delta(\omega)$  [39], which are known functions of wavelength and defined via  $-\alpha_0^{-1} = Z = X + i\delta$ , where  $\alpha_0$  is the polarizability of individual spherical monomers forming the fractal. The formula describing enhancement for RS ( $n = 1$ ) with a large shift and for HRS ( $n = 2, 3, \dots$ ) is as follows [39]:  $G_{fract}^{(n)} \approx [|Z/\delta|^{2n} \delta \text{Im } \alpha(X)] \times [|Z_s/\delta_s|^2 \delta_s \text{Im } \alpha(X(\omega_s))]$ , where  $X_s = X(\omega_s)$ . In this formula,  $\text{Im } \alpha(X)$  is the average absorption by fractals. The formula above is in good agreement with simulations based on numerical solutions of the coupled-dipole equations in fractals [39] and gives an enhancement factor for the HRS ( $n = 2$ ) up to  $10^{10}$  for  $\lambda = 1.5 \mu\text{m}$ . For the three-photon pumped HRS ( $n = 3$ ), the enhancement reaches  $10^{18}$  in the near infrared [39]. In our particular case, for  $n = 2$  and  $\lambda = 0.63 \mu\text{m}$ , this formula gives an enhancement factor of  $10^6$  for HRS.

The microcavity enhancement  $g_{cav}^{(n)}$  depends on whether the fundamental and scattering waves couple to the MDRs of the cavity. Typical quality factors for our microcavities are of the order of  $10^4$  [15]. Thus, even if it is assumed that the cavity enhancement for the two-photon pumped HRS is close to its maximum,  $g_{cav}^{(2)} \sim Q_\lambda^2 Q_{\lambda_s} \sim 10^{12}$ . Combined electromagnetic enhancement from fractal modes and microcavity results in a ratio of hyper-Raman/Raman intensity of  $10^{-6}$ – $10^{-7}$ . Since the experimental spectra contain many anti-Stokes emission peaks whose intensities are approximately equal to the Stokes Raman peak intensities, it is concluded that they cannot arise from hyper-Raman scattering from pure molecular transitions.

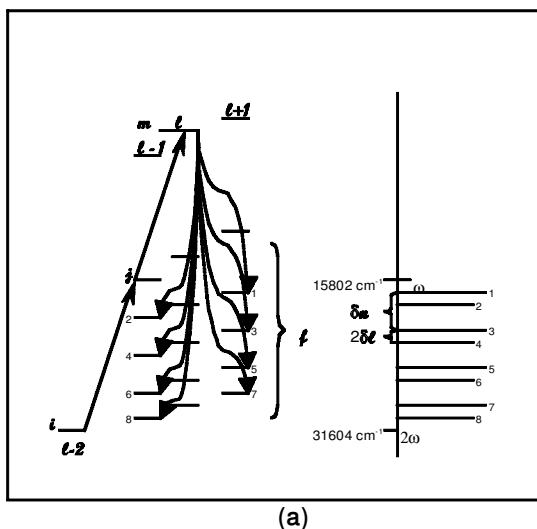
Based on the above considerations, it is suggested that electronic states of metal nanoparticles may play an important role in the observed spectrum. One can model a metal particle as a spherical quantum well and consider linear and nonlinear optical excitations of the electron gas as transitions between the discrete nanoparticle states [16, 40]. The energy  $E_{nl}$  of the states with quantum numbers  $nl$  in a spherical particle of radius  $a$  is given by  $E_{nl} = E_0 \alpha_{nl}^2$ , where  $E_0 = \hbar^2/2ma^2$  and  $\alpha_{nl}$  is the  $(n + 1)$  zeros of Bessel functions of the first kind of half-integer,  $l + 1/2$  order [16]. The characteristic separation of excited levels in a particle of radius  $10 \text{ nm}$  is  $740 \text{ cm}^{-1}$  near the Fermi energy  $E_F$ ; note that these are larger than the relaxation width  $\Gamma$  ( $\sim 100 \text{ cm}^{-1}$ ). Optical response of electrons in the particle contain the Drude part, caused by the nonresonant transitions in a thin energy layer near the Fermi surface, and a resonant (quantum-size) contribution caused by resonant transitions between the discrete states of the finite-size particle. There

are grounds to believe that the Drude part of the field-induced population of excited states is directly transformed (as a result of relaxation) into the quasi-equilibrium distribution, with a certain effective temperature. Relaxation of the resonant part may proceed in a more complicated, multistage way [16], involving electron emission [41] or radiative decay. As is well known for electrons localized inside a metal [17, 18], excited electron states cannot decay via photon emission since such a process cannot simultaneously conserve energy and momentum. In contrast, for rough surfaces, where the translational invariance is broken, photon emission can occur. It is worth mentioning that in the metal the mean free-path of electrons above the Fermi energy exceeds the particle size [42]. Since the electron wavelength in the particle is  $\lambda = \hbar/(2mE_i)^{1/2} = a/\alpha_i$  ( $i = nl$ ) and, above the Fermi energy, is less than  $10^{-2}a$ , particle surface roughness on the scale of interatomic distances becomes important, so that the excited electron can be trapped and spend some time in the surface states. These states are strongly coupled to molecular vibronic transitions because of chemisorption. Surface states can be created by small  $Ag_n$  clusters and cations formed as defects on the particle surface and they can strongly bind molecules.

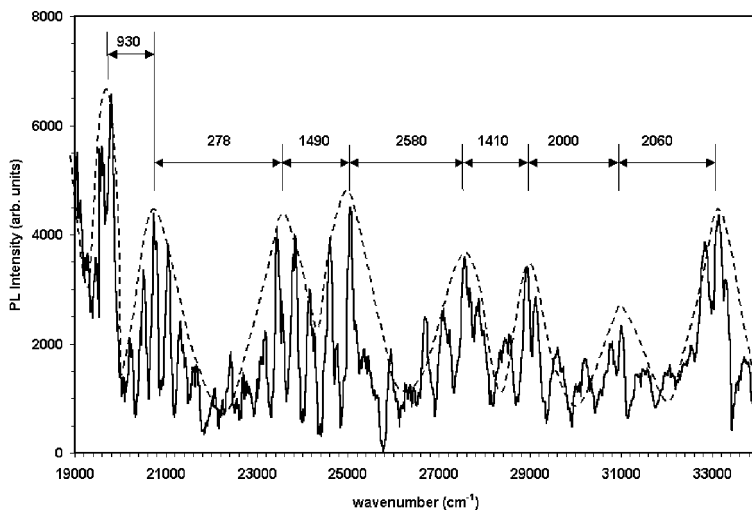
Based on the above considerations, it is suggested that the observed discrete, multiphoton-excited emission spectrum results from a multistage process. An electron excited via a two- or three-photon transition (via steplike or cooperative processes [43]) is first trapped in a surface state. This is followed by emission of a photon after the electron returns to the metal particle, leaving the adsorbate molecule in a vibrationally excited state. Radiative decay of multiphoton excited states may go into many unoccupied electronic states of the metal particle causing a rich discrete spectrum spanning a broad range.

For sodium citrate molecules, minimal energy of the transitions is in the UV region (the absorption band is centred near 220 nm). In this ‘nonresonant’ case it is expected that, for the blue-green spectral region, electron states of the complex are governed by electron states of the metal particle. As shown below, despite the enormous number of possible transitions in a metal particle, spectral lines under two-photon excitation can be resolved, and one can find characteristic scales of the expected spectrum. We consider transitions between electronic states of a metal nanoparticle within the framework of Rautian’s theory [16] and assume, for simplicity, that the surface states make possible the radiation of photons. A sketch of possible transitions for two-photon excited emission is shown in figure 6a, where the curved arrows imply a radiative decay.

According to the quantum well model, the energy of stationary states is governed by  $E_0 = 3.08\text{cm}^{-1}$ , in our case, and by  $\alpha_{nl}$  (which for the possible initial states  $i$  varies from  $((E_F - \hbar\omega)/E_0)^{1/2} \sim 100$  to  $(E_F/E_0)^{1/2} \sim 120$ ). Transitions to possible final states (denoted by  $f$ ) give two characteristic spacings,  $\delta_n = 2E_0\alpha_{nl}\Delta\alpha_n$  ( $\Delta n = 1$ ) and  $2\delta_l = 4E_0\alpha_{nl}\Delta\alpha_l$  ( $\Delta l = 1$ ), where the factor 2 in the last equation is due to the difference in  $l$  for transitions  $\Delta l = \pm 1$ . For states having a large statistical weight  $2(l+1)$ , known properties of zeros of Bessel functions [44] imply for the  $n, l$  interval of interest that  $\Delta\alpha_n(\Delta n = 1) = Q_{nl}$ , where  $4 < Q_{nl} < 7$  and  $\Delta\alpha_l(\Delta l = 1) = P_{nl}$ , with  $1.2 > P_{nl} > 1.03$ . Thus, the estimate for the two characteristic scales of the spectrum is given by  $2700 < \delta_n < 4700 \text{ cm}^{-1}$  and  $1400 < 2\delta_l < 1600 \text{ cm}^{-1}$ . Comparison with the experimental spectrum in the range  $\hbar\omega$  to  $2\hbar\omega$ , presented in figure 6, indicates good agreement between these scales and the observed spacing between the spectral line groups. Whether these



(a)



(b)

Figure 6. (a) Scheme of transitions for two-photon excited emission in metal spherical particle and sketch of expected spectrum (right side). Illustrates a possible set of two-photon excited transitions. Beginning with state,  $i$ , characterized by quantum numbers,  $(n, l-2)$  for this example, the sequential excitation of states,  $j$ ,  $(n+4, l-1)$ , and  $m$ ,  $(n+8, l)$ . Emission then occurs to a number of states, for example, to the state,  $f_1$ ,  $(n+3, l+1)$ . The characteristic spacings,  $\delta_n$ , and  $2\delta_l$ , discussed in the text, are shown. The smallest spacing,  $\Delta_3$  (not shown) is easily reconstructed by beginning the sequence with the next highest (or lowest) initial state. For example, beginning the sequence from the next highest state,  $i$   $(n, l-1)$ , through the intermediate states,  $j$   $(n+4, l)$ ,  $m$   $(n+8, l+1)$ , and emission into the state,  $f_1$   $(n+3, l+2)$ . The difference frequency between this, and the previous transition will be the smallest spectral scale,  $\Delta_3$ . The estimation gives:  $130 < \Delta_3 < 270 \text{ cm}^{-1}$ ,  $1400 < \Delta_2 < 1600 \text{ cm}^{-1}$ ,  $1100 < \Delta_1 < 3300 \text{ cm}^{-1}$ . (b) Fragment of the experimental spectrum from Ag/citrate/tube at 632 nm excitation. The groups of peaks are numbered to illustrate experimental characteristic scales, which are:  $\Delta_1 = 2780, 2580, 2000 \text{ cm}^{-1}$ ;  $\Delta_2 = 930, 1490, 1410, 2060 \text{ cm}^{-1}$ ;  $\Delta_{3avg} = 350 \text{ cm}^{-1}$ .

scales manifest themselves in the spectrum depends on the density of spectral lines.

We estimate now how many transitions are in one-photon resonance with the incident light. The total number of initial states  $N(\alpha, \Delta\alpha)$ , which is governed by the number of pairs  $(n, l)$  satisfying the inequality  $100 < \alpha_{nl} < 120$ , is estimated to be 640 in our case. Each of the states yields only two transitions with the energy closer than  $\delta_n$  to  $\hbar\omega$ , one for  $\Delta l = +1$ , and one for  $\Delta l = -1$ . Therefore, the number of resonant transitions is estimated as  $2N\Gamma/\delta_n \sim 28$  to 46. Using the same analysis, there are only one or two double-resonance transitions that are simultaneously resonant for one- and two-photon energies. Thus, the resonance factor and the weight factor  $2l + 1$  narrow down all possible transitions to roughly one two-photon excited state. The radiative decay of this state gives about  $2\hbar\omega/\delta_n$  intense spectral lines in the  $\hbar\omega$  to  $2\hbar\omega$  region. These lines correspond to the observed maxima of the spectral groups. As is clear from figure 6a, spacing between spectral groups should be  $\Delta_1 = \delta_n - 2\delta_l$  and  $\Delta_2 = 2\delta_l$ . Other spectral lines are quasis resonant and have less intensity. The spacing between the quasis resonant lines should be larger than the difference between energies of the neighbouring transitions (for the initial state  $l$  changes by 1). This gives a third characteristic spacing for the spectra,  $\Delta_3 = 2E_0(\alpha_m - \alpha_f)$ , which is estimated as  $130 < \Delta_3 < 270 \text{ cm}^{-1}$  and exceeds  $\Gamma$  (the experimentally observed average spacing is about  $350 \text{ cm}^{-1}$ ) (see captions of figure 6a,b for more detail). It is concluded that the observed three scales are in a qualitative accord with the experimental spectra. An important consequence of this model is that two-photon excited emission lines can be resolved because of the discrimination resulting from the resonant and statistical weight factors, whereas the one-photon excited emission cannot typically be resolved, because the number of resonant transitions is approximately 15–20 times greater.

A theory of the saturation effect in a metal particle [16] gives the saturation parameter for the resonant part of the induced variation of population in the following form:  $(ea/\hbar\omega)^2 I_0\omega/\Gamma_2$ , where  $\Gamma_2 \sim 100 \text{ cm}^{-1}$  is the polarization relaxation rate. As follows from the above considerations, the local field in fractal-microcavity composites can be enhanced by about  $10^7$ , which gives a saturation parameter of 1.6 for  $2 \text{ W cm}^{-2}$  incident intensity. Thus, it is believed that the quasilinear intensity dependence observed in these experiments results from saturation effects.

To summarize, multiphoton-excited emission from metal particle–adsorbate complexes in experiments with fractal-microcavity composites exhibits unusual features such as a discrete spectrum spanning a broad spectral range and a quasilinear dependence on pump intensity.

The above analysis, which is based on the Rautian theory for the optical properties of a degenerate electron gas in a spherical potential well, suggests that the spectra contain clear fingerprints of the quantum size effects in metal particles. Despite simplification of this model, mentioned in [16], qualitative considerations of the characteristic scales in the emission spectrum and the possibility of resolving the multi-photon spectral lines should remain valid because they result only from level spacing. Indeed, particles with similar size but different shape or surface conditions should have a different spectrum, though they have the same average level spacing [45]. The surface conditions, in general, play an important role since they can facilitate the radiative decay; this problem has yet to be studied. The

quantum size effects in the optics of metal particles, which have been studied since the 1960s [46–48], concerned mainly the size-dependence width of the plasmon peak and absorption in the far-infrared region. The manifestation of discreteness in the multiphoton-excited emission spectra discussed in this paper can be important for advancing our understanding of the quantum size problem.

In conclusion, broad-band emissions under single- and multiphoton excitation from adsorbate/Ag colloidal aggregate/microcavity composites have been studied. The low threshold coherent radiation from dye/Ag/microcavity composites is due to the combined action of fractal nanoresonators and the microcavity. The multiplicative enhancement of optical responses in fractal/microcavity composites facilitates light emission resulting from resonant transitions between discrete states of metal nanoparticles and radiation of the energy stored in the long-living triplet states of dye molecules.

### Acknowledgments

We acknowledge helpful discussions with Professor S. G. Rautian, and V. V. Potapov's help in experiments with a dye laser. This work was supported in part by NSF (DMR-98101183 and DMR-0071901), PRF (35028-AC5), CRDF(RE1-2229), and ARO (DAAG55-98-1-0425).

### References

- [1] FLEISCHMANN, M., HENDRA, P. J., and MCQUILLAN, A. J., 1974, *Chem. Phys. Lett.*, **26**, 163–166.
- [2] CHANG, R. K., and FURTAK, T. E. (eds), 1982, *Surface Enhanced Raman Scattering* (New York: Plenum Press).
- [3] MOSKOVITS, M., 1985, *Rev. Mod. Phys.*, **57**, 783–826.
- [4] CAMPION, A., and KAMPAMPATI, P., 1998, *Chem. Soc. Rev.*, **27**, 241–250.
- [5] CHEN, C. K., DE CASTRO, A. R. B., and SHEN, Y. R., 1981, *Phys. Rev. Lett.*, **46**, 145–148.
- [6] BARANOV, A. V., and BOBOVICH, YA. S., 1982, *JETP Lett.*, **36**, 343–346.
- [7] GOLAB, J. T., SPRAGUE, J. R., CARRON, K. T., SCHATZ, G. C., and VAN DUYN, R. P., 1988, *J. Chem. Phys.*, **88**, 7942–7951.
- [8] KNEIPP, K., KNEIPP, H., ITZKAN, I., DASARI, R. R., and FELD, M. S., 1999, *Chem. Phys.*, **99**, 2957–2975.
- [9] ZIEGLER, L. D., 1990, *J. Raman Spectr.*, **21**, 769–779.
- [10] BARANOV, A. V., BOBOVICH, YA. S., and PETROV, V. I., 1984, *Optika i Spekr.*, **56**, 3–5.
- [11] LOMBARDI, J. R., BIRKE, R. L., LU, T., and XU, J., 1986, *J. Chem. Phys.*, **84**, 4174–4180.
- [12] MICHAELS, A. M., NIRMAL, M., and BRUS, L. E., 1999, *J. Am. Chem. Soc.*, **121**, 9932–9939.
- [13] OTTO, A., MROZEK, I., GRABHORN, H., and AKEMANN, W., 1992, *J. Phys.: Condens. Mater.*, **4**, 1143–1212.
- [14] SHALAEV, V. M., 2000, *Nonlinear Optics of Random Media: Fractal Composites and Metal-Dielectric Films* (Berlin: Springer).
- [15] KIM, W., SAFONOV, V. P., SHALAEV, V. M., and ARMSTRONG, R. L., 1999, *Phys. Rev. Lett.*, **82**, 4811–4814.
- [16] RAUTIAN, S. G., 1997, *Sov. Phys. JETP*, **85**(3), 451–461.
- [17] LAMBE, J., and MCCARTHY, S. L., 1976, *Phys. Rev. Lett.*, **37**, 923–925.
- [18] PERSON, B. N. J., and BARATO, A., 1992, *Phys. Rev. Lett.*, **68**, 3224–3227.
- [19] LEE, P. C., and MEISEL, D., 1982, *J. Phys. Chem.*, **86**, 3391–3395.
- [20] HIRAI, H., 1979, *J. Macromol. Sci.-Chem.*, **A13**, 633–649.
- [21] FRENS, G., and OVERBEEK, TH. G., 1969, *Kolloid Z.Z. Polym.*, **233**, 922–930.

- [22] SHUBIN, V. A., KIM, W., SAFONOV, V. P., SARYCHEV, A. K., ARMSTRONG, R. L., and SHALAEV, V. M., 1999, *J. Lightwave Technol.*, **17**, 2183–2190.
- [23] TZENG, H. M., WALL, K. F., LONG, M. B., and CHANG, R. K., 1984, *Opt. Lett.*, **9**, 499–501.
- [24] BISWAS, A., LATI, H., ARMSTRONG, R. L., and PINNICK, R. G., 1989, *Opt. Lett.*, **14**, 214–216.
- [25] ARMSTRONG, R. L., XIE, J.-G., RUEKGAUER, T. E., and PINNICK, R. G., 1993, *Opt. Lett.*, **18**, 119–121.
- [26] LIN, H.-B., EVERSOLE, J. D., and CAMPILLO, A. J., 1992, *Opt. Lett.*, **17**, 828–830.
- [27] KERKER, M., SHIMAN, O., BUMM, L. A., and WANG, D.-S., 1980, *Appl. Opt.*, **19**, 3253–3255.
- [28] SHIMAN, O., BUMM, L. A., CALLAGHAN, R., BLATCHFORD, C. G., and KERKER, M., 1983, *J. Phys. Chem.*, **87**, 1014–1023.
- [29] KAI, S., CHAOZHI, W., and GUANGZHI, X., 1989, *Spectrochimica Acta*, **45A**, 1029–1032.
- [30] CASTRO, J. L., OTERO, J. C., and MARCOS, J. I., 1997, *J. Raman Spectr.*, **28**, 765–769.
- [31] FANG, Y., 1999, *J. Raman Spectr.*, **30**, 85–89.
- [32] MOSKOVITS, M., and SUH, J. S., 1985, *J. Am. Chem. Soc.*, **107**, 6826–6829.
- [33] STREKAL', N. D., OSKIRKO, V. F., MASKEVICH, A. A., NABIEV, I. R., and MASKEVICH, S. A., 2000, *Optika i Spekr.*, **89**, 949–952.
- [34] PURCELL, E. M., 1946, *Phys. Rev.*, **69**, 681–686.
- [35] DE MARTINI, F., and JACOBVITZ, G. R., 1988, *Phys. Rev. Lett.*, **60**, 1711–1714.
- [36] BENNER, R. E., BARBER, P. W., OWEN, J. F., and CHANG, R. K., 1980, *Phys. Rev. Lett.*, **44**, 475–477.
- [37] LIN, H.-B., EVERSOLE, J. D., and CAMPILLO, A. J., 1992, *Opt. Lett.*, **17**, 828–830.
- [38] CHANG, R. K., and CAMPILLO, A. J. (eds), 1996, *Optical Processes in Microcavities*, (Singapore: World Scientific).
- [39] PODOLSKIY, V. A., and SHALAEV, V. M., 2001, *Laser Phys.*, **11**, 26–30.
- [40] HACHE, F., RICARD, C., and FLYTZANIS, C., 1986, *J. Opt. Soc. Am. B*, **3**, 1647–1655.
- [41] LEHMANN, J., MERSCHDORF, M., PREIER, W., THON, A., VOLL, S., and GERBER, G., 2000, *J. Chem. Phys.*, **112**, 5428–5434.
- [42] QUINN, J. J., 1962, *Phys. Rev.*, **126**, 1453–1457.
- [43] OVSYANKIN, V. V., and FEOFILOV, P. P., 1966, *Sov. Phys. JETP Lett.*, **4**, 317–320; 1967, *Appl. Opt.*, **6**, 1828–1833.
- [44] ABRAMOWITZ, M., and STEGUN, I. A., 1972, *Handbook of Mathematical Functions* (New York: Dover Publications).
- [45] KUBO, R., 1962, *J. Phys. Soc. Jpn.*, **17**, 975–986.
- [46] KAWABATA, A., and KUBO, R., 1966, *J. Phys. Soc. Jpn.*, **21**, 1765–1772.
- [47] GOR'KOV, L. P., and ELIASHBERG, G. M., 1965, *Sov. Phys.-JETP*, **21**, 940–947.
- [48] KREIBIG, U., 1974, *J. Phys. F*, **4**, 999–1014.